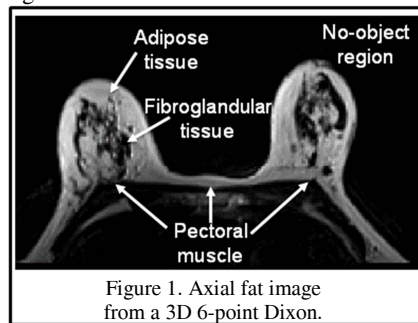


Automatic segmentation of breast images using clustering and dynamic programming

José Angel Rosado-Toro¹, Tomoe Barr², Marilyn T Marron³, Jean-Phillipe Galons⁴, Patricia Thompson³, Alison Stopeck³, Jeffrey Joel Rodríguez⁵, and María I Altbach⁴
¹Electrical and Computer Engineering, University of Arizona, Tucson, Arizona, United States, ²Biomedical Engineering, University of Arizona, Tucson, AZ, United States, ³Arizona Cancer Center, University of Arizona, Tucson, Arizona, United States, ⁴Medical Imaging, University of Arizona, Tucson, Arizona, United States, ⁵Electrical and Computer Engineering, University of Arizona, Tucson, Arizona, United States

Introduction – Breast density (BD) is a known risk factor for the development of breast cancer. BD is routinely measured in mammography by comparing the ratio of stromal tissue to fatty tissue. For longitudinal studies of BD (such as studies involving drugs affecting BD), mammography is not an option due to exposure to ionizing radiation. Moreover, in quantitative studies of BD, mammography has been shown to have poor reproducibility [1]. Dixon-type fat-water MRI methods can be used to obtain quantitative fat-water information on breast images, and parameters derived from the percentage fat distribution have been shown to correlate with mammographic BD [2]. The analysis of data requires delineating ROIs including only the relevant breast anatomy within the images. Since the number of slices to be analyzed is rather large (typically 19 to 48), the segmentation of breast ROIs is a time consuming and tedious process if done manually. In [3] we introduced an automated breast segmentation algorithm in combination with one of the Dixon-type imaging techniques: the radial gradient- and spin-echo (RADGRASE) technique. Here we generalize the algorithm to work with other fat-water imaging techniques suitable for the quantification of BD.



on the fat image, taking advantage of the strong signal intensity gradient between the pectoral muscle (dark) and breast tissue (bright). The *third step* involves removing the skin from the breast ROI using a morphological thinning algorithm. The skin pixels are between the no-object region and the breast tissue and are bright in the water image (not shown) and dark in the fat image. Figure 2 shows how the skin removal technique affects the final segmentation (red is the initial contour; green is the contour after skin removal). A *fourth step* (optional) separates the breast ROI into left and right. This is performed using morphological operations 0.

Methods – The proposed segmentation method can be described in four steps: The *first step* involves the removal of the background (or no-object region). This is performed using k-means++ clustering by grouping pixels in the image into three components (fibroglandular tissue, adipose tissue and background) based on their signal intensity, as shown in Fig. 1. Using a true water or fat image for this step is not always adequate since the signal intensity of adipose tissue in the water image (or fibroglandular tissue in the fat image) may be similar to the no-object region, depending on the imaging technique used. The *second step* consists of finding the pectoral muscle boundary and eliminating all pixels in the image that fall posterior to it. This task is performed

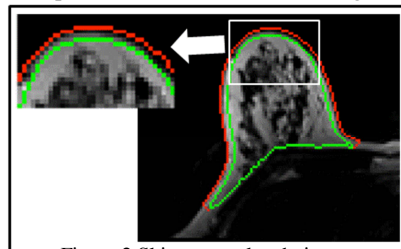
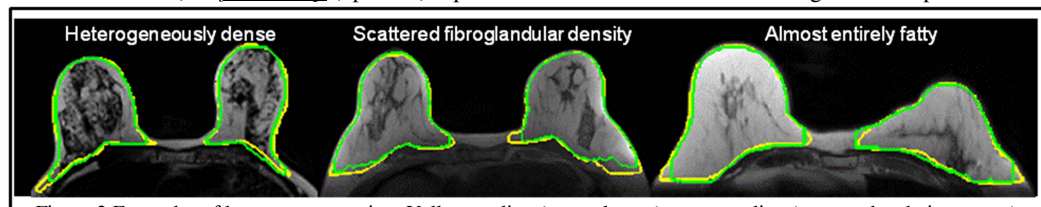


Figure 2. Skin removal technique.



different imaging techniques: a commercially available 3D two-point Dixon method (Siemens 3T Skyra scanner, TR = 6 ms, TE = 1.23 & 2.46 ms, acq. matrix = 384×384, FOV = 38×38 cm; slice thickness = 1.5 mm), a six-point 3D Dixon method (Siemens 3T Skyra scanner, TR = 9.67 ms, TE_s = 1.18, 2.38, 4.76, 5.94, 7.10, 8.26 ms, acq. matrix = 256×122, FOV = 42×25 cm; slice thickness = 4 mm) [4] and a 2D T1-weighted fast spin-echo (FSE) method (GE 1.5T Signa HDxt scanner, TR = 600 ms, TE_{eff} = 8.5 ms, acq. matrix = 256×256, FOV = 34×34 cm; slice thickness = 7 mm). The latter is not a fat-water separation technique since it only yields one image, but these types of images have been used in the literature to threshold fatty pixels based on signal intensity and estimate BD based on the percentage of fatty pixels [5].

The segmentation algorithm described above was used to outline the breast ROI. The automatically segmented ROI was compared to the manual tracing of an experienced tracer using the mean (μ) and standard deviation (σ) of the Dice metric, which is a measure of mutual overlap between the manual and automated segmentation.

Results – Representative images for the three BD categories, together with the automatically segmented (green) and manually traced (yellow) ROIs, are shown in Fig. 3. The Dice metric for the cases shown in Fig. 3 are 0.959, 0.959 and 0.964, respectively. The images shown in Fig. 3 were acquired with 6-point Dixon, 2-point Dixon and T1-weighted FSE, respectively. As shown in Table 1, a mean Dice metric greater than 0.89 was observed for all imaging modalities for 202 breast slices analyzed in the study.

Conclusion – We have presented a technique for the segmentation of breast ROIs generalized to work with a variety of different breast imaging techniques. The technique should significantly reduce the workload for the analysis of BD and other studies that require the segmentation of breast tissue in MRI, such as the segmentation of breast ROIs preceding the automatic segmentation of tumors.

Acknowledgments – T32-HL007955 and R01CA161534.

References:

[1] Ortiz CG, Automatic 3D segmentation of the breast in MRI. M.S. thesis, University of Toronto, 2011; [2] Trouard TP, Proc Int Soc Magn Res Med 2010 4749; [3] Rosado-Toro JA, ICASSP 2013, 1018; [4] Zhong X, MRM, 2014, 72:1353; [5] Khazen M, Cancer Epidemiol Biomarkers 2008, 17.

To evaluate the segmentation performance we use a total of 202 breast image slices from subjects with BD corresponding to the three qualitative categories: almost entirely fatty, scattered fibroglandular densities, and heterogeneously dense. Images were acquired with three

Imaging technique (slices)	Dice metric	
	μ	σ
6-point Dixon (89)	0.917	0.053
2-point Dixon (63)	0.897	0.075
T1- weighted FSE (50)	0.939	0.035

Table 1. Mutual overlap performance